Atmospheric Environment 176 (2018) 261–273

Contents lists available at ScienceDirect

Atmospheric Environment

journal homepage: www.elsevier.com/locate/atmosenv

# Exploratory study of atmospheric methane enhancements derived from natural gas use in the Houston urban area

Nancy P. Sanchez[a,*], Chuantao Zheng[b,c], Weilin Ye[b,d], Beata Czader[a], Daniel S. Cohan[a], Frank K. Tittel[b], Robert J. Griffin[a]

[a] Department of Civil and Environmental Engineering, Rice University, 6100 Main St, Houston, TX, United States
[b] Department of Electrical and Computer Engineering, Rice University, 6100 Main St, Houston, TX, United States
[c] State Key Laboratory on Integrated Optoelectronics, College of Electronic Science and Engineering, Jilin University, 2699 Qianjin Street, Changchun 130012, China
[d] College of Engineering, Shantou University, 243 Daxue Road, Shantou 515063, China

ARTICLE INFO

*Keywords:*
Natural gas
Methane emissions
Natural gas distribution systems
Mobile-mode field monitoring
Thermogenic methane emission sources

ABSTRACT

The extensive use of natural gas (NG) in urban areas for heating and cooking and as a vehicular fuel is associated with potentially significant emissions of methane ($CH_4$) to the atmosphere. Methane, a potent greenhouse gas that influences the chemistry of the atmosphere, can be emitted from different sources including leakage from NG infrastructure, transportation activities, end-use uncombusted NG, landfills and livestock. Although significant $CH_4$ leakage associated with aging local NG distribution systems in the U.S. has been reported, further investigation is required to study the role of this infrastructure component and other NG-related sources in atmospheric $CH_4$ enhancements in urban centers. In this study, neighborhood-scale mobile-based monitoring of potential $CH_4$ emissions associated with NG in the Greater Houston area (GHA) is reported. A novel dual-gas 3.337 μm interband cascade laser-based sensor system was developed and mobile-mode deployed for simultaneous $CH_4$ and ethane ($C_2H_6$) monitoring during a period of over 14 days, corresponding to ~ 90 h of effective data collection during summer 2016. The sampling campaign covered ~250 exclusive road miles and was primarily concentrated on eight residential zones with distinct infrastructure age and NG usage levels. A moderate number of elevated $CH_4$ concentration events (37 episodes) with mixing ratios not exceeding 3.60 ppmv and associated with atmospheric background enhancements below 1.21 ppmv were observed during the field campaign. Source discrimination analyses based on the covariance between $CH_4$ and $C_2H_6$ levels indicated the predominance of thermogenic sources (e.g., NG) in the elevated $CH_4$ concentration episodes. The volumetric fraction of $C_2H_6$ in the sources associated with the thermogenic $CH_4$ spikes varied between 2.7 and 5.9%, concurring with the $C_2H_6$ content in NG distributed in the GHA. Isolated $CH_4$ peak events with significantly higher $C_2H_6$ enhancements (~11%) were observed at industrial areas and locations with high density of petroleum and gas pipelines in the GHA, indicating potential variability in Houston's thermogenic $CH_4$ sources.

## 1. Introduction

Methane ($CH_4$), a potent greenhouse gas (GHG) that also contributes to background ozone levels, is emitted from multiple sources including natural gas (NG) and petroleum systems, mobile and stationary combustion, and microbial degradation in landfills and wastewater treatment plants (EPA, 2017; Fiore et al., 2008). Natural gas systems, including production, processing, and transmission and distribution, constitute the second largest known source of $CH_4$ emissions to the atmosphere, with estimated 6.5 million metric tons $CH_4$ emitted in 2015 (24.8% of total $CH_4$ emissions in the U.S) (EPA, 2017). Ethane ($C_2H_6$), which also contributes to surface ozone formation and impacts the oxidative capacity of the atmosphere, is co-emitted with $CH_4$ derived from NG systems but not from non-fossil sources (Brandt et al., 2016; Helmig et al., 2016; Schoell, 1980; Simpson et al., 2012; Xiao et al., 2008). Considering the impact of $CH_4$ and $C_2H_6$ in the atmosphere, fugitive emissions from NG systems may potentially outweigh the benefits associated with increased NG usage derived from replacement of coal and oil (Brandt et al., 2016).

Despite multiple studies investigating NG leakage occurring in production and processing stages (Allen et al., 2015; Brantley et al., 2014b; Mitchell et al., 2015; Subramanian et al., 2015; Zavala-Araiza et al., 2015), particular uncertainty remains on the extent of $CH_4$ emissions associated with NG distribution systems (NGDS), which

* Corresponding author.
*E-mail address:* nps1@rice.edu (N.P. Sanchez).

https://doi.org/10.1016/j.atmosenv.2018.01.001
Received 15 June 2017; Received in revised form 27 December 2017; Accepted 2 January 2018
Available online 04 January 2018
1352-2310/ © 2018 Elsevier Ltd. All rights reserved.

deliver this fuel to final residential and commercial consumers in urban areas (Hendrick et al., 2016; Jackson et al., 2014). This uncertainty is reflected by differing estimates by the 1990–2010 U.S. GHG inventory (EPA, 2012) and a recent study by Lamb et al. (2015), which based on measurements in thirteen U.S urban distribution systems reported 36–70% lower $CH_4$ emissions from NGDS. Furthermore, the most recent U.S. GHG inventory (EPA, 2017) estimates $CH_4$ emissions from NGDS ~65% lower than the 1990–2013 U.S. GHG inventory for the same period of time (e.g., 2011–2013) (EPA, 2015b, 2017). NGDS have been identified as relevant $CH_4$ emission sources in different U.S. urban areas with reported NG loss rates from local NGDS varying between ~2 and 6%, and nationwide estimates between 0.1 and 0.22% (Cambaliza et al., 2015; Lamb et al., 2015, 2016; McKain et al., 2015; Wennberg et al., 2012).

In the past 60 years, the NGDS infrastructure in the U.S. has evolved from being mainly constituted by leak-prone materials such as unprotected steel (bare steel, BS) and cast iron (CI) to being dominated by plastic pipelines (DOE, 2017; PHMSA, 2016b). Pipeline replacement programs have followed distinct dynamics in different U.S. states, leading to local NGDS with marked differences in pipeline composition and infrastructure age (DOE, 2017; Gallagher et al., 2015). As such, it is expected that leaks from the NGDS are highly spatially dependent.

Recent initiatives such as those of the Environmental Defense Fund and Google Earth Outreach (von Fischer et al., 2017) have conducted $CH_4$ leak surveys in several U.S. urban areas, following previous studies mostly conducted in Northeast and Midwest cities (Chamberlain et al., 2016; Gallagher et al., 2015; Hendrick et al., 2016; Jackson et al., 2014; Lamb et al., 2016; McKain et al., 2015; Phillips et al., 2013). The incidence of $CH_4$ leaks associated with NGDS has been reported as significant for urban centers with aging NG infrastructure including Washington D.C., Boston, MA and New York City, and more moderate for cities such as Durham, NC, Cincinnati, OH and Ithaca, NY (leak densities ranging between 0.22 and 4.3 leaks/road mile) (Chamberlain et al., 2016; Gallagher et al., 2015; Jackson et al., 2014; Phillips et al., 2013). In addition to emissions from local NGDS and end-use uncombusted NG, emissions from compressed NG (CNG) fueled vehicles have been reported as relevant urban sources of atmospheric $CH_4$ (Curran et al., 2014; Hesterberg et al., 2008; Lamb et al., 2016; von Fischer et al., 2017).

The reported variability in NG leakage across the U.S. and the potential occurrence of $CH_4$ emissions from distinct in-use NG sources in urban centers highlight a need for area-specific investigations of enhancements in atmospheric $CH_4$ levels associated with NG distribution and usage. Although the Greater Houston area (GHA) is the fifth-largest metropolitan area in the U.S. and Houston is the most populated center in Texas (which in turn is the largest consumer of NG and has the second largest CNG vehicle fleet in the U.S. (EIA, 2015)), no studies on the occurrence of $CH_4$ emissions associated with the use of NG in this urban center have been reported in the scientific literature to date.

This paper describes an initial study on the incidence of NG-related $CH_4$ emissions in selected zones of the GHA during August and September 2016. Daytime mobile-mode monitoring of $CH_4$ and $C_2H_6$ concentrations was conducted primarily in eight selected residential zones with high, medium and low expected probability of $CH_4$ emissions, according to selected proxies for NGDS infrastructure age and NG usage. Multi-day sampling was performed in zones with higher expected probability of $CH_4$ emissions, while single-day monitoring was conducted in zones with lower potential of $CH_4$ leakage. More limited $CH_4$ and $C_2H_6$ sampling was completed at three GHA neighborhoods with recent reports of NGDS-related incidents associated with pipelines dating back to 1945 (PHMSA, 2016a). Additionally, monitoring of $CH_4$ and $C_2H_6$ levels was conducted continuously while en route to the selected sampling areas. Total monitoring comprised ~90 h of $CH_4$ and $C_2H_6$ concentration data and encompassed approximately 250 exclusive road miles.

$CH_4$ and $C_2H_6$ mixing ratios were measured employing a novel infrared laser-based sensor system developed for simultaneous detection of these gas species based on a single 3.337-μm light source. The compactness of this sensor system, derived mainly from the use of a single laser source and reduced-size electronics, enables its use in mobile-mode environmental monitoring allowing $C_2H_6/CH_4$ ratio-based $CH_4$ source discrimination analyses. While $CH_4$ source profiling based on off-line analysis of ($C_2H_6$ + propane)/$CH_4$ ratios in limited subsets of samples and using the $C_2H_6/CH_4$ ratio employing separate $CH_4$ and $C_2H_6$ instruments has been previously demonstrated (Jackson et al., 2014; Yacovitch et al., 2014), this study reports, for the first time, the application of a single dual-gas instrument enabling continuous $CH_4$ source identification.

## 2. Methods

### 2.1. Selection of sampling zones

Eight residential zones in the GHA with distinct expected probability of NG leakage were selected for monitoring of $CH_4$ and $C_2H_6$ levels. The median housing age (MHA) and the NG heating units density (HUD), as proxies for the NGDS infrastructure age and NG consumption, respectively, were used to define the expected probability of $CH_4$ leakage in the block groups in the GHA (United States Census Bureau, 2014). Four categories of expected $CH_4$ leak occurrence (low, high, medium A and medium B) were defined based on the intersection between MHA and HUD levels as depicted in Fig. 1.

The transition between old and new infrastructure was established based on the predominant pipeline materials used in NG distribution systems over the past 60 years and the tendency of these materials to crack and/or leak (Fig. S1, Supplementary Information, SI). According to the timeline in Fig. S1, pre-1980 and post-1990 block groups in the GHA were classified with higher and lower expected probability of $CH_4$ leakage, respectively (high and medium A, and low and medium B categories in Fig. 1, respectively). This timeline coincides with the approximate transition between metal and plastic pipelines in the Houston area according to non-official information provided by the local NG distribution company (CenterPoint Energy Entex).

Census data from the American Community Survey (United States Census Bureau, 2014) were used to identify neighborhoods in the GHA associated with high density of pre-1980 and post-1990 housing units (above the 90$^{th}$ percentile of the housing unit density in each category for the Houston area). The statistical distribution of the HUD in the preselected zones was examined, and the 10th and 90$^{th}$ percentiles of this

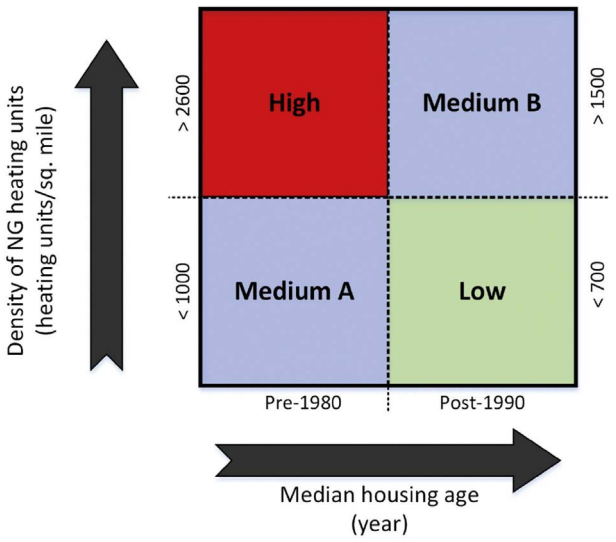


**Fig. 1.** Expected probability of NG leakage based on median housing age and density of NG heating units as proxies for infrastructure age and NG consumption, respectively.

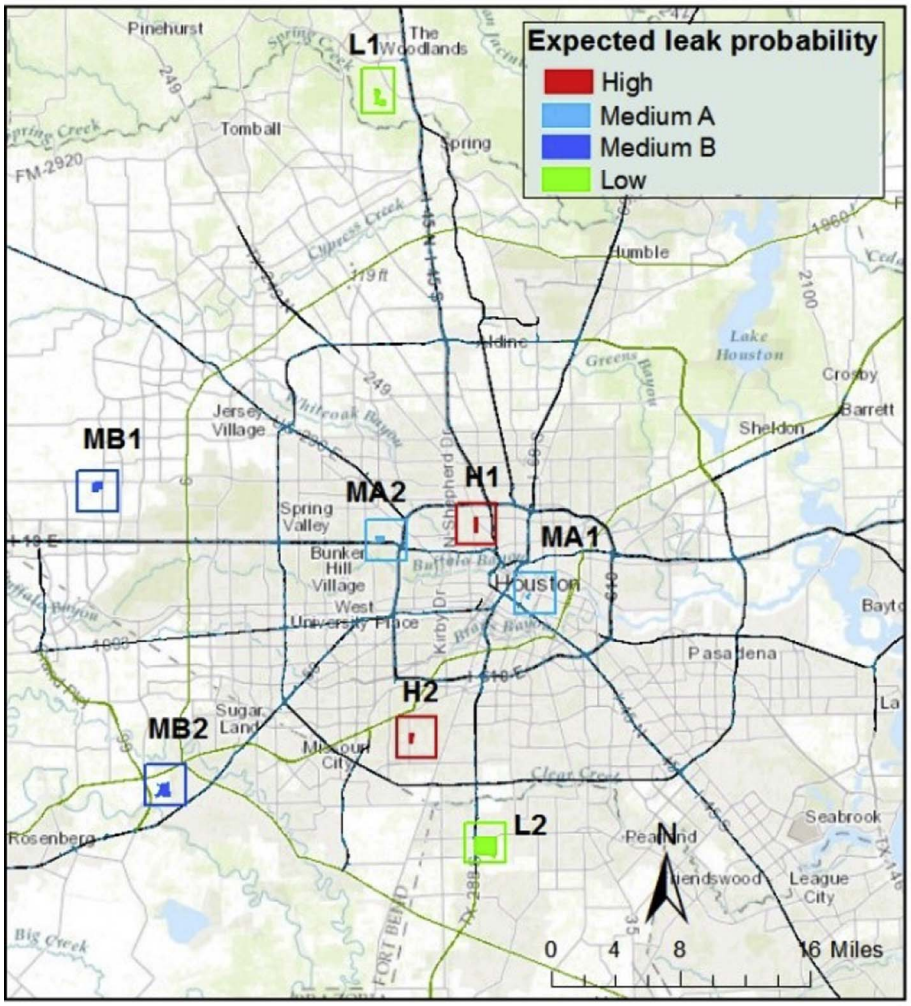


**Fig. 2.** Selected residential sampling zones in the Houston area and expected probability of NG leakage. The characteristics of each zone are presented in Table S1.

variable were used as the upper and lower limit to define zones in the low/medium A and high/medium B probability categories, respectively (Fig. 1). According to these criteria, two residential zones were selected in each category (High: H1 and H2, Medium A: MA1 and MA2, Medium B: MB1 and MB2, and Low: L1 and L2). The location of these zones is presented in Fig. 2 and their characteristics are summarized in Table S1.

In addition to the residential zones selected based on MHA and HUD levels, some areas in the GHA with likely presence of NG aged infrastructure (pre-1980) were identified based on reports of NGDS-related incidents by the local NG distribution Company during 2009–2016 (PHMSA, 2016a). Three neighborhoods (I1, I2 and I3, Fig. S2) with reported incidents involving pre-1980 polyethylene and steel mains and services lines were identified and included in the sampled areas. As no information on the spatial distribution of NGDS pipeline materials in the GHA was accessible, these three zones constitute case studies of interest where (i) some certainty on pipeline type and infrastructure age exists and (ii) NGDS infrastructure failure has occurred. Table S2 presents further information on the NGDS-related incidents reported in these supplementary sampling zones. Although the eight selected zones and supplementary sampling locations corresponded to residential locations with no evident industrial installations, certain areas with high density of industrial facilities and petroleum/gas pipelines outside these zones also were sampled occasionally while en route to/from the selected neighborhoods.

### 2.2. Interband cascade laser-based sensor system for $CH_4$ and $C_2H_6$ detection

A continuous wave (CW) distributed feedback (DFB)-interband cascade laser (ICL)-based sensor system using long-path absorption spectroscopy was developed for the detection of $CH_4$ and $C_2H_6$. This sensor unit employs a single ICL (Nanoplus, Germany) centered at 3337 nm (2996.70 $cm^{-1}$) and simultaneously targets absorption lines at 2999.06 and 2996.88 $cm^{-1}$ for $CH_4$ and $C_2H_6$ detection, respectively (Fig. S3). These absorption lines are not influenced by the presence of typical atmospheric trace gases such as carbon dioxide and nitrous oxide, although potential interference by nearby water absorption lines located at 2998.97 and 2999.16 $cm^{-1}$ can occur (Fig. S3). This potential interaction was addressed by installing a $CaSO_4$-based water trap in the sampling line (Drierite, 8 mesh, W.A. Hammond Drierite Co, LTD, OH).

The ICL was coupled into a compact multipass gas cell (MPGC) (Sentinel Photonics-Aeris Technologies, CA) with an absorption path length of 54.6 m. The output of the MPGC was measured using a mercury-cadmium-telluride infrared detector (PVI-4TE-3.4, Vigo Systems, Poland) with optimal detection at 3400 nm. A temperature controller (model 0520, Wavelength Electronics, MT) and a reduced-size custom laser current driver were used for the ICL operation. The ICL beam pattern in the MPGC mirror surfaces was adjusted by using a visible diode laser beam (wavelength 630 nm, Coherent Inc., CA) co-aligned with the ICL until a non-overlapping dense pattern in the MPGC was obtained.

Wavelength modulation spectroscopy with second harmonic (2*f*

signal) detection was implemented by employing LabVIEW-based ICL wavelength scan, function generator, signal acquisition module and lock-in amplifier software. These signals were transmitted via a DAQ card (NI USB-6356, National Instruments). Dual gas detection was realized by applying a current range between 31 and 49 mA to the ICL while operating at 10 °C. A flowmeter (M-2SLPM-D, Alicat Scientific, Inc, AZ), pressure controller (649A, MKS Instruments, Inc, MA) and vacuum pump (N 813.5 ANE/AF, KNF Neuberger Inc, NJ) formed the sampling component of the sensor unit. The sensor architecture is presented in Fig. S4.

The sensor system was operated at 100 Torr and calibrated using different concentrations of $CH_4$ and $C_2H_6$ obtained by dilution of standard gas cylinders (2.1 ppmv and 1.14 ppmv for $CH_4$ and $C_2H_6$, respectively) employing an automated gas dilution system (series 4040, Environics, Inc, CT). Linear response (2*f* signal) of the sensor system at different concentrations of $CH_4$ and $C_2H_6$ was observed as illustrated in Fig. S5. The stability of the response of the sensor unit was examined at different concentration levels of $CH_4$ (0, 300, 600 and 900 ppbv) and $C_2H_6$ (0, 30, 60 and 90 ppbv). Relative standard deviations between 2.6 and 5.3% and 3.0 and 9.4% for $CH_4$ and $C_2H_6$, respectively, indicated relatively minor fluctuation at the evaluated conditions.

Further evaluation of the stability and precision of the output from the sensor system was conducted using an Allan-Werle variance analysis. Results of this analysis using pure $N_2$ (Cao et al., 2015) indicated minimum sensor system detection levels of 17.4 and 2.4 ppbv for $CH_4$ and $C_2H_6$, respectively, for an averaging time of 4.3 sec. The response time of the sensor system, defined as the time required to rise from 10% to 90% and to fall from 90% to 10% of the final concentration for increasing/decreasing concentration steps, was ~90 sec, as illustrated in Fig. S6. Thus, although the ICL-based sensor unit allows effective detection of $CH_4$ and $C_2H_6$ concentration enhancements during field measurements, short-term concentration fluctuations of these gas species (< 90 sec) might not be fully captured by the instrument and associated time delays might exist when monitoring $CH_4$ and $C_2H_6$ spikes. The performance of the dual-gas sensor unit for laboratory and short-term stationary atmospheric monitoring was previously evaluated, and sensitive simultaneous detection of $CH_4$ and $C_2H_6$ was demonstrated, indicating its suitability for studying the incidence of NG-related $CH_4$ atmospheric enhancements. The results of these tests, as well as detailed information on the sensor operation and development process, were reported previously (Ye et al., 2016).

### 2.3. Sensor deployment and field campaign

The incorporation of a LabVIEW lock-in amplifier and reduced-size electronics to replace bulky commercial devices traditionally employed, as well as the use of a single ICL for dual gas detection, led to the compact field-deployable sensor system presented in Fig. S7. As observed in Fig. S7, an aluminum enclosure was installed in the optical core of the sensor unit to protect its optical components and reduce the potential impact of characteristic high ambient humidity levels present in the Houston area during summer. After weatherization, the $CH_4$ and $C_2H_6$ sensor system was deployed in a gasoline mid-size passenger vehicle for mobile-mode monitoring of these trace gases in the GHA during summer 2016.

A set of high capacity rechargeable batteries (PG-12V150-FG, Power-sonic Corporation, CA) and a DC to AC inverter (Model 9622, Wagan Coporation, CA) were used to supply power to the components of the sensor system during mobile deployment. A Teflon filter (pore size 1.0 μm, PALL Corporation, NY) was installed at the entrance of the sampling line to prevent particle flow to the MPGC. This filter and the desiccant employed in the water trap were replaced daily. A Teflon sampling line (1/8 in), located ~ 1 m above ground level and positioned ahead of the vehicle exhaust in order to prevent any self-sampling, was used for introducing the sampled gas to the MPGC. A weather station with an integrated 10 Hz GPS (Airmar 150WX) was installed on the roof of the vehicle and employed for acquiring ambient temperature, barometric pressure, vehicle geographical coordinates and apparent/true wind speed and direction while sampling. A single data file containing the Airmar 150WX data output as well as the sensor system output (i.e. $CH_4$ and $C_2H_6$ 2*f* signals and concentrations) at unified time stamps was generated every ~5 sec during each field test (Table S3). The in-motion noise floor of the sensor system during field deployment was evaluated and compared with noise levels observed during typical laboratory measurements, as illustrated in Fig. S8. As shown in this Figure, similar noise levels of ~20 and 1.2–2 ppbv for $CH_4$ and $C_2H_6$ detection, respectively, were observed for field and laboratory operation, indicating minor impact of mobile mode-related factors (e.g., vibration and vehicle movement) on the sensor unit response. This instrument noise level is sufficient for detecting typical NGDS-related leaks, which according to previous reports usually involve atmospheric $CH_4$ enhancements exceeding ~700 ppbv, and only few instances with leaks associated with concentration spikes below 150 ppbv (Jackson et al., 2014; Phillips et al., 2013; Chamberlain et al., 2016; Gallagher et al., 2015). Additional information on the mobile sampling configuration is presented in Table S3.

Calibration of the sensor system was conducted on a regular basis during the field campaign using standard gas cylinders of $CH_4$ (2.1 ppmv) and $C_2H_6$ (1.14 ppmv). Mobile-mode monitoring of $CH_4$ and $C_2H_6$ concentration levels was conducted during 14 days encompassing ~90 h of sampling in the selected residential zones (vehicle speed below 15 mph) and while driving to/from these areas (vehicle speed below 30 mph). Additionally, less intensive monitoring was conducted in the three neighborhoods corresponding to likely pre-1980 NG infrastructure (I1-I3, Fig. S2). Table S4 summarizes the frequency, times and duration of sampling, as well as the road miles covered at the eight selected residential zones during the field campaign. As shown in this Table, sampling in the H1, H2, MA and MA2 zones (i.e., zones with higher expected probability of $CH_4$ leakage based on infrastructure age) was conducted in a multi-day basis, alternating between morning and afternoon periods. Sampling in the zones with more recent infrastructure (MB1, MB2, L1 and L2) was performed at a single instance with longer duration than the daily monitoring in the multi-day sampling scheme (Table S4). As shown in Table S4, monitoring was conducted only during daytime (~10:00–17:00 CST), covering similar periods in each zone. At each selected location, transects were monitored repeatedly by driving the entire area of the neighborhood multiple times. The approximate 90 h of field sampling covered an area of ~250 exclusive miles (i.e., not including repeated sampling on the same roads), from which about 98 road miles were driven in the selected residential zones and supplementary sampling locations I1, I2 and I3 (Tables S4 and S5). The remaining over 150 miles corresponded to roads covered while en route to/from the selected sampling locations. The sampling/driving time, monitoring dates and number of driving cycles in these roads are presented in Fig. S9 and Table S6.

### 2.4. Peak identification and source discrimination methods

Sustained increases in $CH_4$ concentration exceeding by three standard deviations the atmospheric $CH_4$ background level were considered as $CH_4$ peak events. This peak identification criterion was equivalent to the definition of peaks based on concentration increases over the 90$^{th}$ percentile of the observed $CH_4$ mixing ratios for a monitoring interval. The background concentration of $CH_4$ for a particular period was calculated as the 5th percentile of the corresponding concentration time series (Brantley et al., 2014a; Bukowiecki et al., 2002).

The likely origin of the observed $CH_4$ peaks (e.g., thermogenic versus biogenic) during the field campaign was determined based on the slope of the orthogonal regression (OR) between $CH_4$ and $C_2H_6$ concentrations levels during the concentration spikes (Yacovitch et al., 2014). The slope of the OR represents the $C_2H_6$ enhancement (%v/v) in the detected $CH_4$ peaks and thus provides information on the nature of

the source associated with the detected increase in $CH_4$ concentration. $C_2H_6$ is primarily absent from $CH_4$ emitted from biogenic sources and therefore constitutes a marker of $CH_4$ derived from thermogenic sources (Hausmann et al., 2016; Schoell, 1980). Additionally, the intercept of a Keeling-like plot (KLP), which equally provides the $C_2H_6/CH_4$ ratio in a $CH_4$ peak by paralleling $C_2H_6$ to a $CH_4$ isotope, was calculated for comparison purposes (Yacovitch et al., 2014). $CH_4$ concentration peak events with statistically significant association ($p < .01$) between $CH_4$ and $C_2H_6$ mixing ratios and coefficients of correlation (R) above 0.7 were related with thermogenic sources. Peak events with no statistically significant association or low R levels between $CH_4$ and $C_2H_6$ concentrations were categorized as likely of biogenic origin. For these peaks, the upper limit of the 95% confidence interval of the OR slope was reported as an estimate of the maximum $C_2H_6$ volumetric content in the potential emission source (Yacovitch et al., 2014).

## 3. Results and discussion

### 3.1. Inter and intra-neighborhood variation in $CH_4$ concentration

The spatial variation of the $CH_4$ mixing ratios in each selected zone during the field campaign is presented in Fig. 3, while the associated zonal concentration statistics are summarized in Table S7. Fig. 3 presents multi and single-day sampling concentration data for H1/H2/MA1/MA2 and L1/L2/MB1/MB2, respectively. For the zones in which multi-day sampling was conducted (H1/H2/MA1/MA2), Table S8 shows slight variability between the mean $CH_4$ mixing ratios in each neighborhood (relative standard deviations (RSD) of 3.0, 3.99, 1.78 and 0.26% in H1, H2, MA1 and MA2, respectively). Table S8 also indicates minor differences between the mean $CH_4$ mixing ratios for morning and afternoon sampling hours in the distinct zones (variability < 5%). This observation is consistent with sampling being conducted after development of the boundary layer, and concurs with results on the diurnal dynamics of $CH_4$ mixing ratios previously reported by our research group, which indicate that after a significant increase in concentration occurring in the early morning, a variation below 4% was observed for the $CH_4$ levels between 10:00 and 18:00 CST (Dong et al., 2016). As presented in Fig. 3, atmospheric $CH_4$ concentrations in the selected neighborhoods ranged between 1.89 and 3.57 ppmv, with larger levels observed in the zones with high expected probability of $CH_4$ leakage (H1 and H2). The mean $CH_4$ mixing ratio followed the sequence H1 > H2 > MA1 > L2 > MA2 > MB2 > L1 > MB1, with higher variability present in H1 and H2, as reflected by larger RSD levels (Table S7).

The meteorological conditions during sampling at each zone are summarized in Table S4, and the zonal variability in wind speed (WS) levels is illustrated in Fig. S10. As presented in Fig. S10, relatively consistent WS levels were observed in the distinct neighborhoods, with mean WS varying between 1.37 and 1.92 m/s (associated RSD: 11.8%). As shown in Table S4, similar zonal WS distributions were observed during sampling, with levels below 2 m/s being predominant across the selected zones. Additionally, as sampling was conducted during similar daytime hours, comparable ambient temperatures (90.6–97.6 °F), were recorded during monitoring (Table S4), reinforcing the presence of fairly consistent meteorological conditions during the field campaign. Based on WS levels, sky cover and solar elevation angles during sampling, it was established that atmospheric turbulence levels corresponded primarily to Pasquill stability classes A and B (extremely and moderately unstable, respectively - Table S4) (Turner, 1994), suggesting, as discussed in the SI (including Tables S9 and S10), that similar zonal pollutant dispersion dynamics was likely present during the field monitoring (Beychok, 2005). Considering the relatively consistent meteorology in the course of the field campaign, it is expected that the $CH_4$ concentration comparison presented in Fig. 3 and summarized by the H1 > H2 > MA1 > L2 > MA2 > MB2 > L1 > MB1 sequence represents the inter-zone variability in $CH_4$ mixing ratios during the sampling period. In order to further examine this hypothesis, the potential impact of the WS levels on this concentration trend during sampling was examined by analysis of covariance (ANCOVA) (SPSS 20.0, IBM Corp., Armonk, NY) (Table S11), as described in the SI. The mean $CH_4$ mixing ratio adjusted by the effect of WS, as resulting from ANCOVA, are included in Table S7. As indicated by these results, minor variations (not exceeding 0.17%) can be noticed between the mean and adjusted mean $CH_4$ concentrations in each zone, indicating that the sequence above also represents the zonal $CH_4$ mixing ratios trends while accounting for WS during sampling. Additional details on the ANCOVA application are provided in the SI.

An inverse significant linear relationship between MHA and the mean concentration of $CH_4$ in the selected zones ($R = -0.76$, $p < .05$) was observed, suggesting higher atmospheric levels of this gas species in neighborhoods with older infrastructure. As recently constructed neighborhoods tend to be located in more outlying zones of the GHA, the significant inverse association between MHA and $CH_4$ levels could reflect this fact. The co-linearity between block group's MHA and its distance from downtown Houston ($R = 0.92$ and $R = 0.53$, $p < .01$ for the eight selected zones and for 2523 block groups within 35 miles from the center of Houston, respectively) support this observation.

One-way analysis of variance (Minitab 17, Minitab Inc., PA) indicated statistically significant differences ($p < .01$) between the average $CH_4$ concentrations in the distinct residential zones, pointing out noticeable inter-neighborhood variation in $CH_4$ levels. Differences between zones with high, medium (A and B), and low expected probability of NG leakage were examined by linear discriminant analysis (LDA) (SPSS 20.0, IBM Corp., Armonk, NY) using $CH_4$ and $C_2H_6$ mixing ratios as the discriminating variables. Two canonical discriminant functions (F1 and F2) accounting for 66.1 and 33.9% of the discriminating ability of the $CH_4$ and $C_2H_6$ concentrations, respectively, were obtained. $CH_4$ concentration is highly correlated with F1, while F2 exhibits high association with $C_2H_6$ concentrations (i.e. greater impact of $CH_4$ and $C_2H_6$ levels on F1 and F2 discriminant scores, respectively, Tables S12 and S13). The higher discriminating capability accounted by F1 is reflected by the larger difference in the mean of the F1 scores (functions at group centroids, Table S14) between the High, Medium A, Medium B and Low zones compared with the corresponding difference for F2. The mean of the scores for F1 differs particularly for the High and Low zones, with more moderate differences between the Medium A/Medium B and High/Low zones (Table S14). The F1 and F2 discriminant scores for the distinct zones (Fig. S11) show that the High, Medium A and Low leakage probability zones can be differentiated primarily based on F1, while unclear differentiation of Medium B from the other zones can be noticed based on F1 and F2 scores (number of Medium B data points classified correctly by LDA was ~41%, Table S15).

The intra-neighborhood spatial variation of $CH_4$ mixing ratios was also examined by applying the Anselin Local Moran's I statistics (Spatial Statistical tools, ArcMap 10.1, ESRI, CA) at each sampling location (intra-zone clusters). The H1, H2, MB2 and L2 zones were characterized by clusters of high $CH_4$ concentration (HH) disperse across the sampling areas, while HH clusters were more grouped at H2, MA1 and L1, and nearly absent from MB1 (Fig. S12). The maximum $CH_4$ concentration of the observed HH clusters in the selected residential zones ranged between 2.16 and 3.57 ppmv, with the largest levels observed in the H2 and MA2 zones (Table S16). Further details on the Anselin Local Moran's I statistics for cluster analysis and LDA application are provided in the SI.

Potential differences in the type of $CH_4$ sources impacting the selected zones during the monitoring period were investigated based on the correlation between $C_2H_6$ and $CH_4$ mixing ratios at each location. Significant association between $C_2H_6$ and $CH_4$ levels ($p < .01$) with coefficients of correlation above 0.6 was noticed in the MA2 and L1 zones (Fig. 4), indicating probable influence of thermogenic $CH_4$ sources in these areas. $C_2H_6/CH_4$ ratios of 3.3 ± 0.10% and

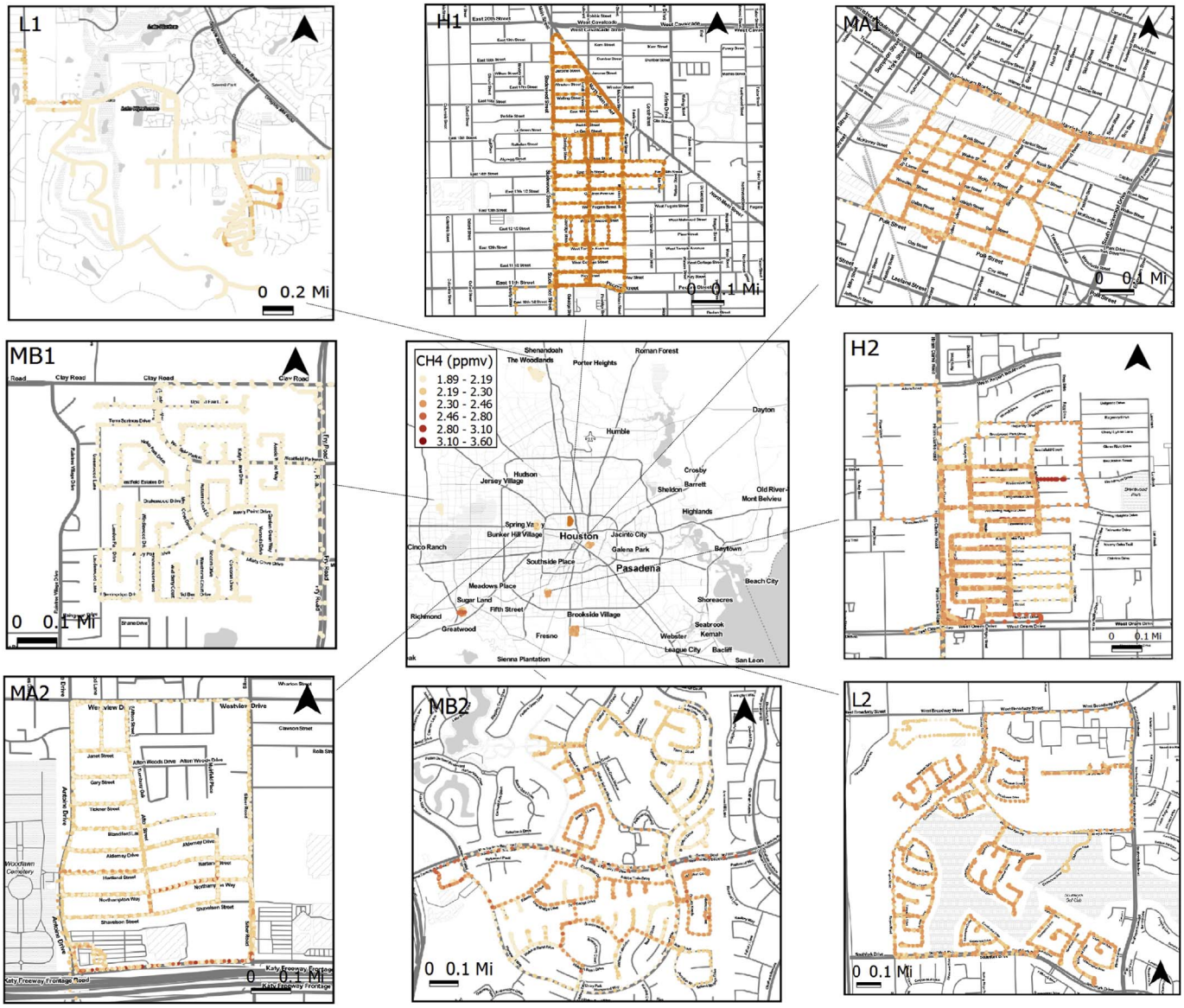


**Fig. 3.** Spatial variation of $CH_4$ mixing ratios in the GHA residential zones selected for monitoring during summer 2016. Color scale in ppmv is included in the central map of the Figure. Mixing ratios correspond to data collected while driving in each sampling zone. For H1, H2, MA1 and MA2 the mapped $CH_4$ mixing ratios include multiple days of sampling, while concentrations mapped for MB1, MB2, L1 and L2 correspond to single-day monitoring (Table S4). The variation in $CH_4$ concentrations in zones where multi-day sampling was conducted (H1/H2/MA1/MA2) is presented in Table S8. Mean $CH_4$ mixing ratios and background levels (5th percentile of the collected concentration data) in each zone are shown in Table S7. Meteorological conditions present during each sampling instance are included in Table S4. Darker points in zones such as H2, MA2 and L1 correspond to detected $CH_4$ peak events, while darker coloration in zones such as H1 and MA1 mostly reflect overall larger atmospheric $CH_4$ levels not evidently associated with peak occurrences (Section 3.3). Potential time delay in concentration data due to the specific sensor system time response is not reflected in this Figure. (For interpretation of the references to color in this figure legend, the reader is referred to the Web version of this article.)

1.9 ± 0.13% (slope of the OR between $C_2H_6$ and $CH_4$ concentrations ± standard error) for MA2 and L1, respectively, agreed well with the fraction of $C_2H_6$ in NG distributed in the Houston area (Section 3.3).

In contrast, the H1, H2 and MB1 zones were characterized by nearly null association ($p < .01$) between $CH_4$ and $C_2H_6$ levels, suggesting minor influence of $CH_4$ thermogenic sources during the sampling period. Although the $C_2H_6$ and $CH_4$ concentrations were significantly correlated ($p < .0.1$) in the MA1 and MB2 areas, lower R levels were observed in these zones (0.57 and 0.41, respectively).

As shown in Fig. 4, two distinct trends between $C_2H_6$ and $CH_4$ mixing ratios were observed in L2. While null correlation between $C_2H_6$ and $CH_4$ concentrations was observed during the major portion of the sampling interval, the influence of $CH_4$ sources was reflected by a $C_2H_6/CH_4$ ratio of 14 ± 0.8% detected during a fraction of the monitoring period. This large $C_2H_6/CH_4$ ratio was associated with an increase in $CH_4$ and $C_2H_6$ mixing ratios observed across the L2 area for a ~1h sampling period. As no significant differences in wind patterns occurred during this episode and the remaining sampling interval at L2, potential $CH_4$ sources other than NGDS leakage (which would be observed consistently) are considered. Large $C_2H_6/CH_4$ molar ratios (~0.164) have been reported for emissions derived from biomass burning during open cooking (Akagi et al., 2011), and biomass burning has been identified as a relevant source of atmospheric $CH_4$ and $C_2H_6$ by previous studies (Aydin et al., 2011; Kirschke et al., 2013; Xiao et al., 2008). Considering that the observed episode occurred while sampling at lunchtime during a summer holiday weekend (9/3/2016) and that the wind was blowing predominantly from the Northeast where a nearby major public park is located, biomass burning related with open cooking is hypothesized as a potential $CH_4$ source at L2.

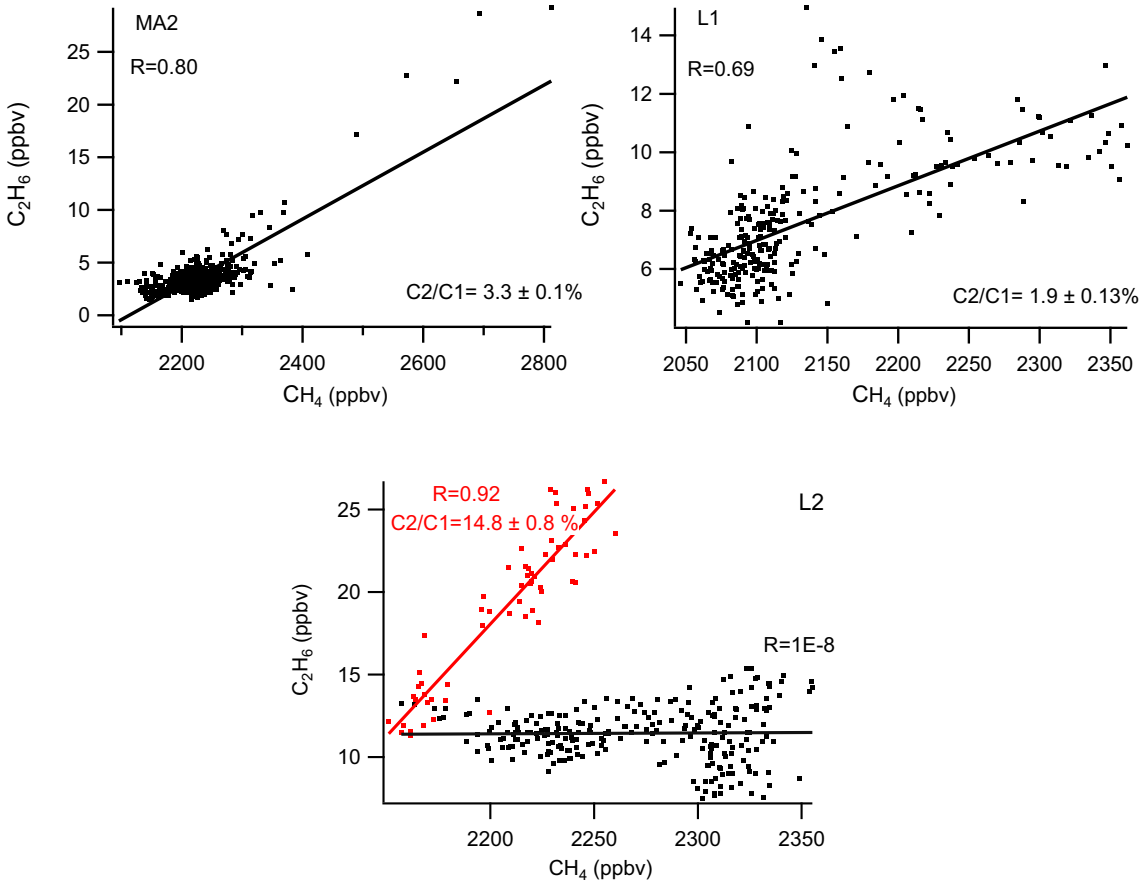


**Fig. 4.** 60-sec average mixing ratios of $CH_4$ and $C_2H_6$ in residential zones where statistically significant association ($p < .01$) and coefficients of correlation > 0.6 were observed between these trace gases during the sampling period. C2/C1 corresponds to the slope of the orthogonal regression between $C_2H_6$ and $CH_4$ concentrations. The slope ± associated standard error is reported in each case. The two slopes shown for the L2 sampling are described in the text.

### *3.2. Spatial variation of $CH_4$ mixing ratios in the Houston area*

Spatial averages (100 × 100 m) of the $CH_4$ mixing ratios measured during the entire field campaign (Fig. 5) showed a variation between 1.87 and 3.57 ppmv in $CH_4$ levels across the Houston area. As illustrated by Fig. S13, measured $CH_4$ mixing ratios were mainly concentrated in the 2.02 and 2.37 ppmv range with only some instances above 2.40 ppmv ($90^{th}$ percentile of the 100 × 100 m averages). Higher $CH_4$ concentrations (2.40–3.60 ppmv, Fig. 5) were mostly observed in the central, central west and central south parts of Houston, with some large levels detected in the east region of the GHA. Although limited in temporal and geographical coverage, Fig. 5 suggests a gradient in $CH_4$ concentrations with lower levels in north and west peripheral locations. This observation is consistent with differences above 160 ppbv in the estimated $CH_4$ background levels (computed as the 5th percentile of the $CH_4$ concentration times series at each sampling zone, Table S7) observed between perimetric Houston areas (e.g., MB1 and L1) and more central GHA locations (e.g., H1 and H2).

The presence of clusters of high $CH_4$ concentration across the GHA was examined by applying the Anselin Local Moran's I statistics on the 100 × 100 m averaged data. Six major regions of HH clusters (CR1 to CR6) mainly located in the central (including the H1 zone) and west central parts of Houston were identified during the sampling period (Fig. 6).

The association between $C_2H_6$ and $CH_4$ mixing ratios in the cluster regions was examined to gain insight into the influence of different types of $CH_4$ sources during the sampling intervals at these locations. No statistically significant association ($p > .01$) or low correlations ($R < 0.4$) between $C_2H_6$ and $CH_4$ levels were observed at CR1, CR3, CR4 and CR5, and thus the upper limit of the 95% confidence interval of the $C_2H_6/CH_4$ ratios is reported for these locations in Fig. 6. As illustrated in this Figure, two trends in the correlation between $C_2H_6$ and $CH_4$ concentrations were observed in CR2 and CR6. CR2 exhibited a $C_2H_6/CH_4$ ratio < 0.05% ($R = 0.23$) in most of its area and a larger ratio of 1.5 ± 0.32% ($R = 0.63$) in the northern segment of the cluster region. Significant association ($p < .01$, $R > 0.75$) between $C_2H_6$ and $CH_4$ levels were noticed at CR6 with $C_2H_6/CH_4$ ratios of 2.5 ± 0.21% and 5.7 ± 0.73% for the two segments encompassed by the cluster (Fig. 6). The $C_2H_6/CH_4$ ratios in the detected cluster regions suggest predominant impact of biogenic $CH_4$ sources in CR1 to CR4 during the sampling period and point out NG-related sources of $CH_4$ likely impacting CR6 and a minor portion of CR2 (according to data on the $C_2H_6$ content in NG distributed in the GHA, Section 3.3). No conclusive inference on the character of potential sources influencing CR5 was possible as the upper limit of the 95% confidence interval of the $C_2H_6/CH_4$ ratio in this region comprises both biogenic and thermogenic patterns.

Probable $CH_4$ sources associated with the established HH cluster regions include distinct bayous located near CR1 to CR4, as well as petroleum and gas pipelines present in the area encompassed by CR6. Specifically, CR1 and CR2 are located in the perimeter of Brays Bayou with CR2 closely paralleling the course of this water body in this area (Fig. S14). Similarly, White Oak and Buffalo Bayous near CR3 and CR4 might be related with the high $CH_4$ concentration clusters detected at these locations (Fig. S14). The role of water bodies as $CH_4$ emitters to the atmosphere has been studied previously, and $CH_4$ plumes originating from stagnant water in the Houston area have been reported in a recent publication (Stanley et al., 2016; Yacovitch et al., 2014).

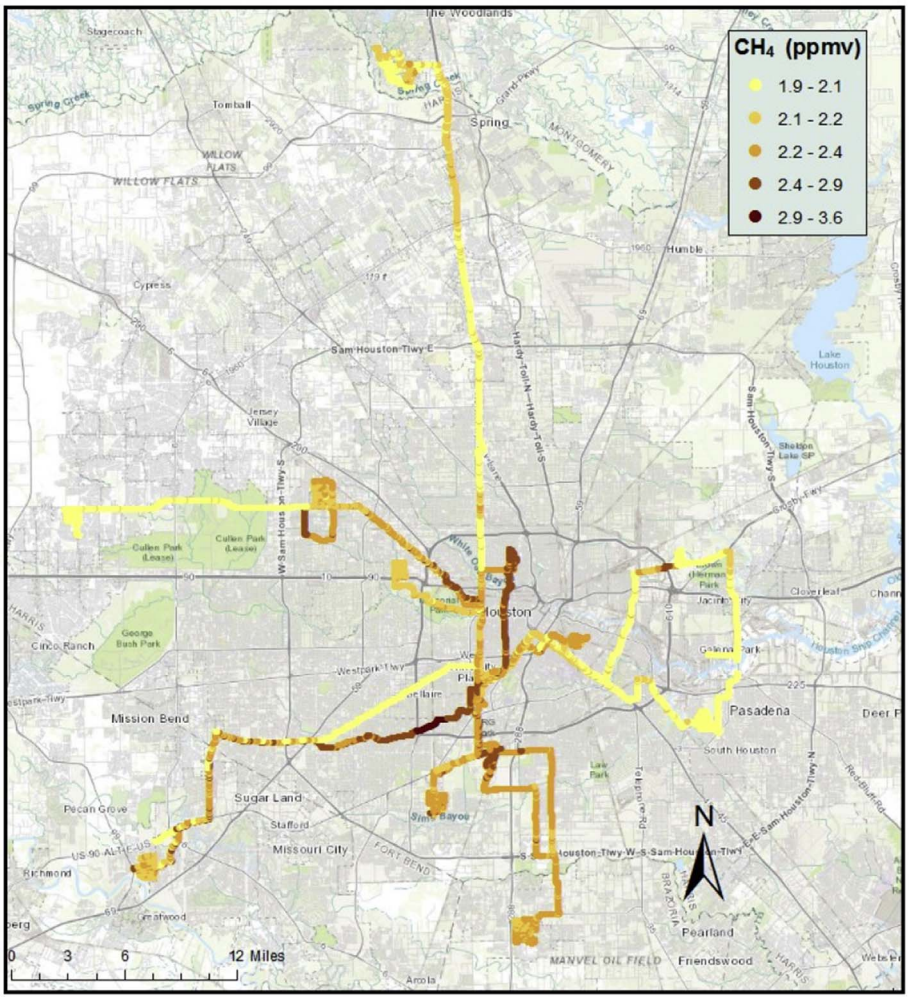


**Fig. 5.** Spatial variation (100 × 100 m averages) of $CH_4$ mixing ratios in the Houston area during the field campaign conducted in summer 2016. Potential time delay in concentration data due to the specific sensor system time response is not reflected in this Figure.

### 3.3. $CH_4$ concentration peak events

A total of thirty-seven events of increased $CH_4$ concentration with maximum levels not exceeding 3.60 ppmv (mean 2.62 ± 0.33 ppmv) were detected during the field campaign.

Twenty of these $CH_4$ spikes had durations below 10 min (median of the peak $CH_4$ concentration episodes), while the remaining concentration peaks (17) were associated with increased $CH_4$ levels lasting between ~12 and 40 min, resembling large-area concentrations enhancements rather than $CH_4$ concentration peak events (Table 1 and Table S17). It is worth noting here that as the likelihood of peak detection and associated peak concentrations likely are influenced by specific meteorological conditions, the results reported in Table 1 and Table S17 primarily reflect emission detection capabilities for predominantly unstable atmospheric conditions as the ones present during the sampling intervals (Pasquill stability classes A and B - Table S4). The spatial distribution of the shorter $CH_4$ concentration increases (i.e., peaks events < Roman > = < /Roman > 10 min) observed during the sampling period are presented in Fig. 7, while the location of the large-area concentration spikes is presented in Fig. S15.

The central, west central and east central areas of Houston contained most of the detected peaks, which exhibited enhancements in $CH_4$ background levels ranging between 138 and 803 ppbv (mean 368 ± 190 ppbv) and maximum $CH_4$ concentrations below 2.93 ppmv. The maximum observed $CH_4$ and $C_2H_6$ concentrations and associated background enhancements at each peak event are summarized in Table 1. The OR and KLP were fit on the $CH_4$ and $C_2H_6$ mixing ratios during the concentration peaks, as illustrated in Fig. S16. These calculation approaches produced similar estimates of the $C_2H_6$ content for most of detected peak events, with values generally differing within 5% except for episodes 13 and 17, which varied by ~35% (Table 1). The probable causes of these differences are discussed later in this Section. Based on the OR and KLP results, 18 of the observed short-term $CH_4$ concentration spikes were likely of thermogenic origin, while biogenic sources were associated with two peak events exhibiting not statistically significant relationships between $CH_4$ and $C_2H_6$ (Table 1).

The location of the $CH_4$ peaks identified as likely biogenic/thermogenic as well as the maximum detected concentration at each peak event are presented in Fig. 7. As shown in Table 1, nine of the detected peaks were located in the selected residential zones, with eight thermogenic peak events detected at MA2 and one likely biogenic $CH_4$ concentration peak observed at L1. The $CH_4$ peak events detected at MA2 and the corresponding OR and KLP for a selected concentration spike are presented in Fig. S17. No $CH_4$ peak events were detected in the high (H1 and H2) and medium B (MB1 and MB2) zones, and no evident correlation between the expected probability of NG leakage (defined based on MHA and HUD) and the number of thermogenic $CH_4$ peak occurrences at the selected residential zones was observed during the sampling campaign. Furthermore, no $CH_4$ peak events were detected in the supplementary residential sampling zones (I1 to I3) where aged NGDS infrastructure is likely present.

The OR-based content of $C_2H_6$ peak events related with thermogenic sources (Events 1 to 18 in Table 1) ranged between 2.9 and 17.0%(v/v), with most of the peaks falling in the 2.9–4.9% region. The spatial distribution of the $C_2H_6$ volumetric fractions in the likely thermogenic concentration peaks is illustrated in Fig. 8. The range of $C_2H_6$

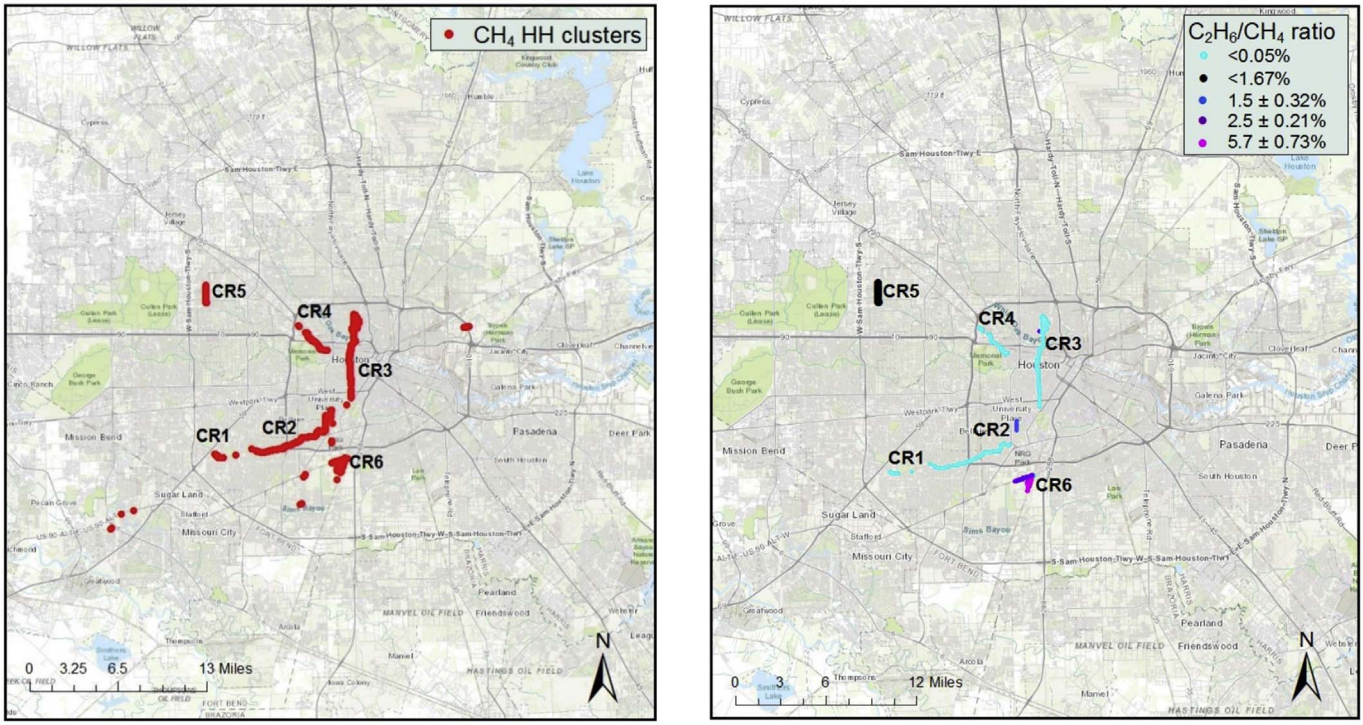


**Fig. 6.** Clusters of high $CH_4$ concentration and $CH_4/C_2H_6$ ratio for major cluster regions identified within the areas sampled in the GHA. $CH_4/C_2H_6$ ratio were derived from orthogonal regression between the mixing ratios of these trace gases. Clusters were defined based on the Anselin Local Moran's I statistics-Spatial Statistical tools (ArcMap 10.1, ESRI, Redlands, CA).

concentration in most of the thermogenic $CH_4$ peaks (2.9–4.9%) overlaps with the $C_2H_6$ content of NG distributed in the Houston area, which according to a recent report, varies between 1.05 and 10.4% (Eastern Research Group, 2012). Furthermore, the potential association of these peak events with NG leakage is reinforced by the consistency between the $C_2H_6$ content range in the observed $CH_4$ peaks and (i) the NG $C_2H_6$ fraction estimated based on the gross heat content of the NG delivered to consumers in Texas during 2016 ($C_2H_6$ ranging between 2.5 and 3.4%, assuming $CH_4$ and $C_2H_6$ as the predominant NG constituents) and (ii) the $C_2H_6$ volumetric content of pipeline quality NG typically transported in local NGDS (< 10%) (EIA, 2016; Michot Foss, 2004).

Two $CH_4$ concentration peaks with larger $C_2H_6$ enhancements were observed while driving in areas with large concentration of chemical/petrochemical facilities and petroleum and gas pipelines (Events 13 and 17 in Table 1). The $C_2H_6/CH_4$ ratios of these peak events were calculated as 16.9 and 17.0% based on OR and as ~10.8 and 11% based on the KLP and ordinary least-squares linear regression (OLR). Considering that the OR and KLP methods are reported to differ when low increases in $CH_4$ levels occur during peak events, as well as the agreement between OLR and the KLP approach, the lower $C_2H_6$ enhancement levels are reported for these peak episodes (Yacovitch et al., 2014). Regardless of the calculation approach used to determine the $C_2H_6/CH_4$ ratio in these peak episodes, these incidences appear to differ in nature/source from the rest of thermogenic peaks detected in the GHA.

Although evident $CH_4$ peak events were only observed at MA2 and L1, large-area $CH_4$ concentration increases spanning between 12 and 47 min occurred in H1, H2, MA1, MA2 and L1 during the sampling period (Table S17). The number of longer $CH_4$ concentration spikes in the selected zones followed the trend H2 > MA2 > MA1 > H1 ~ L1 and involved maximum $CH_4$ mixing ratios between 2.26 and 3.57 ppmv (mean 2.72 ± 0.39 ppmv), with the largest $CH_4$ peak detected at H2 during collection of residential solid wastes by a waste management vehicle on 8/5/2016. This observation is consistent with previous reports on large $CH_4$ concentration peaks associated with the transit of waste collection vehicles in the GHA during summer 2013 (Jahjah et al., 2014).

The association between $CH_4$ and $C_2H_6$ levels during the observed large-area $CH_4$ concentration increases indicates primary influence of biogenic $CH_4$ emission sources in ~80% of these episodes (14) and the potential impact of thermogenic sources in the remaining three instances (with $C_2H_6/CH_4$ ratios varying between 2.9 and 5.9%) (Table S17). Although the $C_2H_6$ content of 16 thermogenic peak events and three large-area concentration episodes indicates their likely association with the NG consumed in the GHA, their connection to leakage from the local NGDS requires further consideration. Previous studies have reported that due to the pressurized character of NGDS, leaks from this infrastructure component usually are observed consistently while repeatedly sampling at a specific location, and that the associated concentration spikes generally extend over short distances (< 160 m) even at high emission rates (von Fischer et al., 2017). In this study, repeated sampling at different days/times conducted at the locations of peak events 1 to 9 (MA2 and a location near Rice University, Table 1 and Fig. 7) indicated that these concentration spikes were not recurrent. Although from these episodes, peaks 2, 6 and 9 (Table 1) were observed for distances shorter than 160 m, the sporadic occurrence of these events necessitates consideration of sources other than NGDS leaks. From the remaining seven peak events, all except peak 15 (Table 1) spanned distances above 160 m, and while dispersion of the plumes can potentially contribute to further extension of the elevated $CH_4$ concentrations, the frequency of sampling at these episode locations is insufficient to determine their potential recurrence.

For comparison purposes, a crude estimate of the upper limit of the leak density for the sampled Houston area can be obtained by assuming that all the observed short-term thermogenic peak events correspond to NGDS leaks. Based on this supposition, an upper limit of 0.08 leaks/mile is calculated, which is an order of magnitude lower than the NG leak incidence reported for cities such as Durham, NC and Ithaca, NY (Chamberlain et al., 2016; Gallagher et al., 2015) and two orders of magnitude lower than the NG leak density observed in Washington D.C. and Boston, MA (Jackson et al., 2014; Phillips et al., 2013). Although, the contrast between the observations from this study and previous reports for other urban centers might be influenced to some extent by

**Table 1**
$CH_4$ concentration peak events (duration ≤ 10min) observed during the field campaign conducted in the Houston area during summer 2016. OR-orthogonal regression, KLP- Keeling-like plot, B-biogenic, T-thermogenic. *significant at α 0.01. SE− standard error of the OR slope. The upper limit of the 95% confidence interval for the $C_2H_6/CH_4$ ratio is reported for coefficients of correlation < 0.6. No sampling zone is reported for $CH_4$ spikes detected in the driving path toward/from the selected residential zones. Location of the peak events is presented in Fig. 7.

| Event ID | Date | Sampling zone | Duration (min) | Maximum $CH_4$ concentration (ppmv) | Maximum $C_2H_6$ concentration (ppbv) | $\Delta CH_4$ (ppbv) | $\Delta C_2H_6$ (ppbv) | $C_2H_6$-$CH_4$ correlation coefficient | $C_2H_6/CH_4$ ratio ± SE (OR slope (%)) | $C_2H_6/CH_4$ ratio ± SE (KLP intercept (%)) | Likely origin |
|---|---|---|---|---|---|---|---|---|---|---|---|
| 1 | 8/9/2016 | | 10 | 2.76 | 22.28 | 467.31 | 20.32 | 0.93* | 3.9 ± 0.15 | 3.9 ± 0.14 | T |
| 2 | 8/11/2016 | MA2 | 8 | 2.53 | 13.12 | 367.32 | 11.76 | 0.61* | 2.7 ± 0.35 | 2.6 ± 0.36 | T |
| 3 | 8/24/2016 | MA2 | 5 | 2.93 | 37.20 | 802.89 | 36.43 | 0.99* | 4.6 ± 0.14 | 4.6 ± 0.12 | T |
| 4 | 8/24/2016 | MA2 | 5.5 | 2.81 | 34.71 | 679.13 | 33.94 | 0.99* | 4.9 ± 0.11 | 4.8 ± 0.12 | T |
| 5 | 8/24/2016 | MA2 | 4 | 2.57 | 19.83 | 437.72 | 19.06 | 0.97* | 4.6 ± 0.15 | 4.5 ± 0.17 | T |
| 6 | 8/24/2016 | MA2 | 4 | 2.35 | 10.38 | 225.66 | 9.61 | 0.80* | 2.7 ± 0.32 | 2.6 ± 0.30 | T |
| 7 | 8/24/2016 | MA2 | 4 | 2.43 | 15.23 | 304.68 | 14.46 | 0.89* | 3.9 ± 0.37 | 3.8 ± 0.33 | T |
| 8 | 8/24/2016 | MA2 | 4 | 2.39 | 11.25 | 260.31 | 10.48 | 0.80* | 3.2 ± 0.32 | 3.0 ± 0.34 | T |
| 9 | 8/24/2016 | MA2 | 3 | 2.37 | 11.27 | 242.27 | 10.50 | 0.68* | 2.8 ± 0.53 | 2.7 ± 0.52 | T |
| 10 | 8/29/2016 | | 8 | 2.46 | 10.93 | 137.87 | 7.32 | 0.57* | 3.1 ± 0.46 | 2.9 ± 0.44 | T |
| 11 | 8/29/2016 | | 9.5 | 2.68 | 16.23 | 287.82 | 12.09 | 0.78* | 3.9 ± 0.28 | 3.7 ± 0.30 | T |
| 12 | 9/3/2016 | | 7 | 2.50 | 29.77 | 258.05 | 16.14 | 0.76* | 3.7 ± 0.42 | 3.5 ± 0.37 | T |
| 13 | 9/3/2016 | | 5.5 | 2.40 | 23.64 | 148.42 | 19.17 | 0.70* | 17.0 ± 2.22 | 11.0 ± 1.47 | T |
| 14 | 9/3/2016 | | 5 | 2.78 | 20.92 | 482.64 | 17.70 | 0.70* | 3.5 ± 0.44 | 3.2 ± 0.47 | T |
| 15 | 9/6/2016 | | 9 | 2.55 | 19.85 | 560.28 | 17.74 | 0.73* | 3.0 ± 0.24 | 2.8 ± 0.25 | T |
| 16 | 9/6/2016 | | 7 | 2.56 | 28.82 | 571.86 | 26.70 | 0.77* | 4.5 ± 0.43 | 4.2 ± 0.40 | T |
| 17 | 9/6/2016 | | 9.1 | 2.21 | 32.09 | 206.54 | 29.60 | 0.69* | 16.9 ± 1.77 | 10.8 ± 1.14 | T |
| 18 | 9/6/2016 | | 10 | 2.27 | 16.76 | 228.78 | 14.65 | 0.79* | 4.8 ± 0.38 | 4.5 ± 0.35 | T |
| 19 | 9/7/2016 | | 8 | 2.59 | 17.56 | 531.62 | 14.91 | 0.14 | < 0.10 | < 0.13 | B |
| 20 | 9/8/2016 | L1 | 8 | 2.19 | 11.84 | 150.41 | 9.19 | 0.24 | < 0 | < 0 | B |

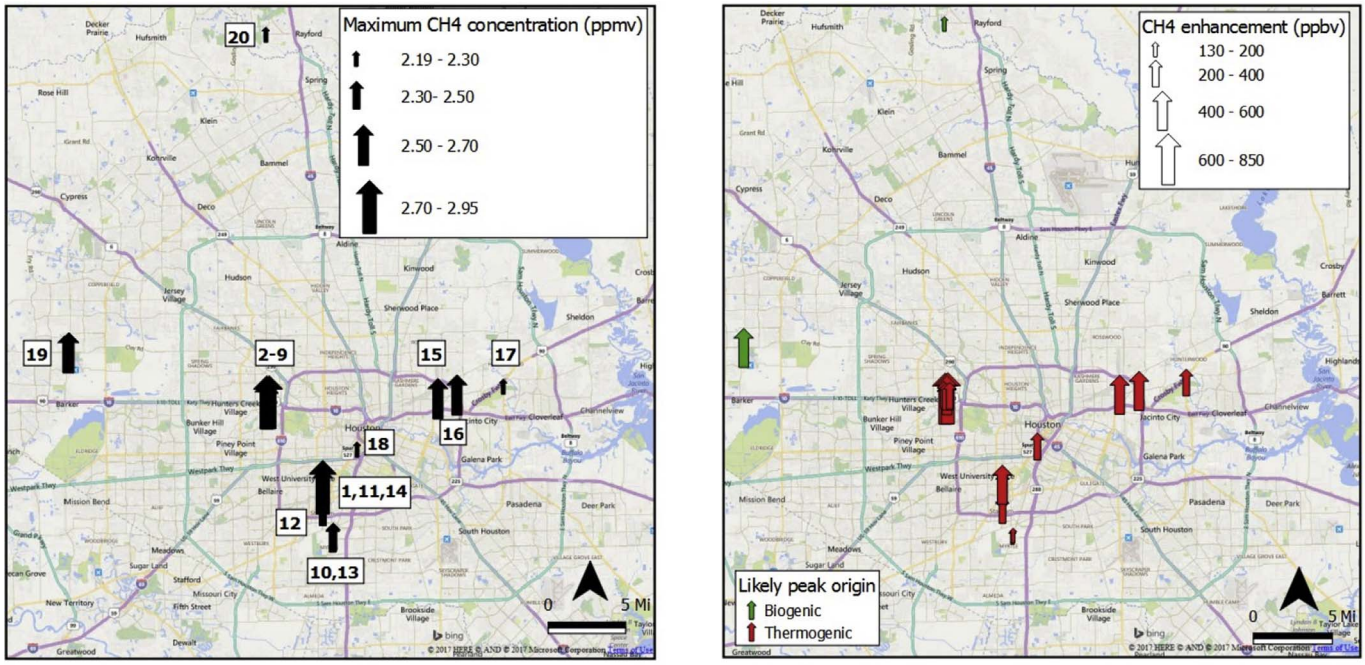


**Fig. 7.** Location and likely origin of $CH_4$ peak events observed in the GHA during the field campaign conducted in summer 2016. The background enhancement and maximum $CH_4$ concentrations associated with the detected elevated concentration episodes are presented. Peak numbers correspond to peak IDs presented in Table 1.

the predominance of unstable atmospheric conditions during sampling in the GHA, it is also likely associated with differing NG infrastructure age, variations in the proportion of BS and CI pipelines in the NGDS and local NGDS operative conditions (e.g., infrastructure maintenance programs). Fig. S18 illustrates the number of BS and CI service lines and distribution mains miles reported by the local NG distribution company operating in Houston, Boston, MA and Washington, D.C. to the Pipeline and Hazardous Materials Safety Administration in 2016 (EPA, 2013,

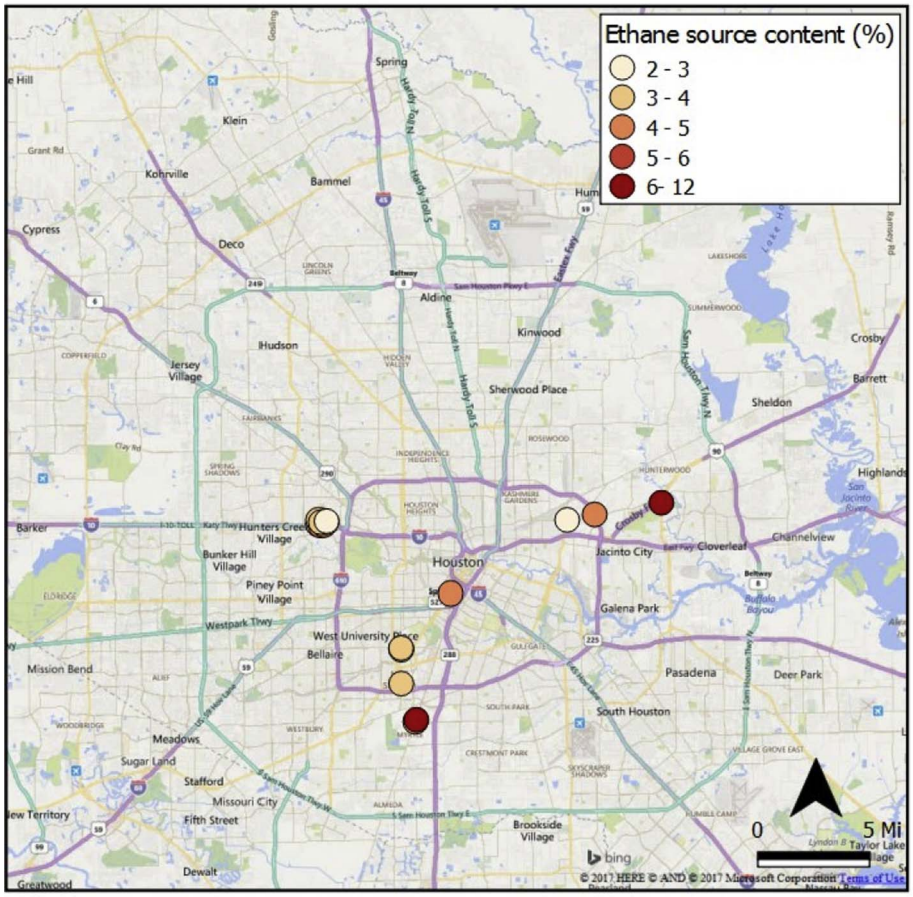


**Fig. 8.** Spatial distribution of $C_2H_6$ content in thermogenic peaks identified during sampling in the GHA in summer 2016.

2015a; PHMSA, 2016b). According to Fig. S18, CI pipelines are nearly absent from the Houston NG distribution system, and the combined BS and CI distribution mains miles in Washington, D.C. and Boston, MA, are four and sixteen times larger than those present in Houston, respectively. Similarly, the aggregated BS and CI service line count follows the ratio trend 37:3:1 between Boston, MA, Washington, D.C. and Houston. It is worth noting that although the GHA constitutes a large proportion of the area covered by the respective local NG distribution company, the data reported by this Company also include locations in east and south Texas, indicating that the actual ratios between BS and CI pipelines in the three urban centers are likely larger than the estimations presented above (EPA, 2013).

During the sampling campaign, MA2 was the only selected residential zone where thermogenic peak events with a signature reflecting the composition of NG distributed in the GHA were observed. This zone, contrasting with the rest of selected sampling areas, is characterized by its proximity to a major highway (Katy Freeway). The location of the $CH_4$ concentration peaks observed in MA2 and the wind patterns during their occurrence are presented in Fig. S19. Similar wind direction and atmospheric turbulence levels were present during the sampling periods where no $CH_4$ concentration spikes were detected in this zone (Table S4), suggesting that the sources associated with these spikes were not permanently situated at the same location. As illustrated in Fig. S19, the peak events in the MA2 zone were mostly observed on main roads and in the proximity of the Katy Freeway, with the highest $CH_4$ concentrations detected during episodes 3 and 4 (Table 1), which were located on the service road of the Freeway. These observations, as well as southerly winds consistently blowing during the peak episodes, suggest the potential association of these elevated concentration events with mobile sources fueled by NG. This hypothesis is consistent with previous observations on major expected incidence of elevated $CH_4$ concentration episodes related with CNG vehicles on high traffic density roadways (von Fischer et al., 2017).

## 4. Conclusions

Monitoring of atmospheric $CH_4$ and $C_2H_6$ mixing ratios conducted in the GHA during August and September 2016 indicated clear differences in $CH_4$ concentrations across selected sampling areas, with levels varying between 1.89 and 3.60 ppmv. Regions with clusters of large $CH_4$ concentration influenced by biogenic and thermogenic $CH_4$ sources mainly were observed in the central, west and southwest parts of the Houston area. Similar meteorological conditions were present during sampling in the selected zones, with wind speeds primarily below 2 m/s and extreme/moderate unstable atmospheric conditions consistently present during the field campaign. Thirty-seven incidences of elevated $CH_4$ concentration were detected during the sampling campaign in the GHA. Twenty of these incidences were classified as peak events (duration $<$ 10 min), while the remaining instances ($\sim$12–40 min) were considered as large-area concentration episodes. These large area concentration increases were primarily related with biogenic sources, as indicated by the lack of correlation between their $CH_4$ and $C_2H_6$ levels. Sixteen peak events and three large-area concentration episodes were related with thermogenic sources exhibiting a $C_2H_6$ content ranging between 2.9 and 5.9% (v/v), which agree with the composition of the NG distributed in the Houston area. Repeated monitoring at the locations of nine of the thermogenic $CH_4$ peak events indicated that leakage from the NGDS was potentially out of consideration as a likely source of these episodes. From the remaining peak incidences (7), six episodes were observed over distances above a reference span reported for NGDS leaks ($<$ 160 m), and while dispersion of the plumes can potentially contribute to further extension of the elevated $CH_4$ concentrations, the frequency of sampling at these locations was insufficient to establish a potential link between the NGDS and the detected episodes. Overall, no evident correlation between the expected probability of NG leakage (based on MHA and HUD) and the number of detected thermogenic events in the selected residential zones was observed. The largest density of thermogenic $CH_4$ peak events occurred in a west Houston neighborhood characterized by its proximity to a major highway. The spatial distribution of the increased concentration episodes in this zone, as well as the predominant wind direction during their occurrence, suggest the influence of NG fueled vehicles on the concentration spikes observed in this area. Further study would be required to confirm this hypothesis. Additionally, two $CH_4$ concentration peaks with large $C_2H_6$ enhancements differing from the bulk of observed thermogenic episodes were observed at locations with large concentration of chemical/petrochemical facilities and petroleum and gas pipelines, indicating potential variability in the thermogenic $CH_4$ sources impacting the GHA. Although, the observations from this study indicate that leakage from the NGDS in the GHA might be less frequent and of lower intensity compared to U.S. urban centers with more prevailing aged infrastructure, it is worth noting that these results reflect emission detection capabilities for predominantly unstable atmospheric conditions. Thus, long-term studies accounting for meteorological variation are needed to evaluate comprehensively the incidence of NG-related atmospheric $CH_4$ enhancements in the GHA.

## Acknowledgments

This work was conducted with support from the Rice University Shell Center for Sustainability and two DOE ARPA-E awards (DE-0000545, DE-0000547). Nancy Sanchez and Robert Griffin acknowledge support from the George R. Brown School of Engineering at Rice University. The authors thank Dr. Christian Davies from Shell Oil Company for valuable discussion and insight on the field component of this study.

## Appendix A. Supplementary data

Supplementary data related to this article can be found at http://dx.doi.org/10.1016/j.atmosenv.2018.01.001.

## References

Akagi, S.K., Yokelson, R.J., Wiedinmyer, C., Alvarado, M.J., Reid, J.S., Karl, T., Crounse, J.D., Wennberg, P.O., 2011. Emission factors for open and domestic biomass burning for use in atmospheric models. Atmos. Chem. Phys. 11, 4039–4072. http://dx.doi.org/10.5194/acp-11-4039-2011.

Allen, D.T., Pacsi, A.P., Sullivan, D.W., Zavala-Araiza, D., Harrison, M., Keen, K., Fraser, M.P., Daniel Hill, A., Sawyer, R.F., Seinfeld, J.H., 2015. Methane emissions from process equipment at natural gas production sites in the United States: pneumatic controllers. Environ. Sci. Technol. 49, 633–640. http://dx.doi.org/10.1021/es5040156.

Aydin, M., Verhulst, K.R., Saltzman, E.S., Battle, M.O., Montzka, S.A., Blake, D.R., Tang, Q., Prather, M.J., 2011. Recent decreases in fossil-fuel emissions of ethane and methane derived from firn air. Nature 476, 198–201. http://dx.doi.org/10.1038/nature10352.

Beychok, M.R., 2005. Fundamentals of Stack Gas Dispersion. published by author, Irvine, CA. fourth ed. .

Brandt, A.R., Heath, G.A., Cooley, D., 2016. Methane leaks from natural gas systems follow extreme distributions. Environ. Sci. Technol. 50, 12512–12520. http://dx.doi.org/10.1021/acs.est.6b04303.

Brantley, H.L., Hagler, G.S.W., Kimbrough, E.S., Williams, R.W., Mukerjee, S., Neas, L.M., 2014a. Mobile air monitoring data-processing strategies and effects on spatial air pollution trends. Atmos. Meas. Tech. 7, 2169–2183. http://dx.doi.org/10.5194/amt-7-2169-2014.

Brantley, H.L., Thoma, E.D., Squier, W.C., Guven, B.B., Lyon, D., 2014b. Assessment of methane emissions from oil and gas production pads using mobile measurements. Environ. Sci. Technol. 48, 14508–14515. http://dx.doi.org/10.1021/es503070q.

Bukowiecki, N., Dommen, J., Prévôt, A.S.H., Richter, R., Weingartner, E., Baltensperger, U., 2002. A mobile pollutant measurement laboratory—measuring gas phase and aerosol ambient concentrations with high spatial and temporal resolution. Atmos. Environ. 36, 5569–5579. http://doi.org/10.1016/S1352-2310(02)00694-5.

Cambaliza, M.O.L., Shepson, P.B., Bogner, J., Caulton, D.R., Stirm, B., Sweeney, C., Montzka, S.A., Gurney, K.R., Spokas, K., Salmon, O.E., Lavoie, T.N., Hendricks, A., Mays, K., Turnbull, J., Miller, B.R., Lauvaux, T., Davis, K., Karion, A., Moser, B., Miller, C., Obermeyer, C., Whetstone, J., Prasad, K., Miles, N., Richardson, S., 2015. Quantification and source apportionment of the methane emission flux from the city of Indianapolis. Elementa Science of the Anthropocene 3, 000037. http://dx.doi.org/10.12952/journal.elementa.000037.

Cao, Y., Sanchez, N.P., Jiang, W., Griffin, R.J., Xie, F., Hughes, L.C., Zah, C.-e., Tittel, F.K., 2015. Simultaneous atmospheric nitrous oxide, methane and water vapor detection with a single continuous wave quantum cascade laser. Opt. Express 23, 2121–2132. http://dx.doi.org/10.1364/oe.23.002121.

Chamberlain, S.D., Ingraffea, A.R., Sparks, J.P., 2016. Sourcing methane and carbon dioxide emissions from a small city: influence of natural gas leakage and combustion. Environ. Pollut. 218, 102–110. http://dx.doi.org/10.1016/j.envpol.2016.08.036.

Curran, S.J., Wagner, R.M., Graves, R.L., Keller, M., Green Jr., J.B., 2014. Well-to-wheel analysis of direct and indirect use of natural gas in passenger vehicles. Energy 75, 194–203. http://dx.doi.org/10.1016/j.energy.2014.07.035.

DOE, 2017. Natural Gas Infrastructure Modernization Programs at Local Distribution Companies: Key Issues and Considerations. Office of Energy Policy and Systems Analysis, Washington, D.C, pp. 78. https://energy.gov/epsa/downloads/natural-gas-infrastructure-modernization-programs-local-distribution-companies-key.

Dong, L., Li, C., Sanchez, N.P., Gluszek, A.K., Griffin, R.J., Tittel, F.K., 2016. Compact $CH_4$ sensor system based on a continuous-wave, low power consumption, room temperature interband cascade laser. Appl. Phys. Lett. 108, 011106. http://dx.doi.org/10.1063/1.4939452.

Eastern Research Group, 2012. Condensate Tank Oils and Gas Activities. Final Report. . https://www.tceq.texas.gov/assets/public/implementation/air/am/contracts/reports/ei/5821199776FY1317-20130831-erg-upstream_oil_gas_heaters_boilers.pdf.

EIA, 2015. Natural Gas Annual Report. Office of Oil, Gas, and Coal Supply Statistics, Washington, DC. . https://www.eia.gov/naturalgas/annual/pdf/nga15.pdf.

EIA, 2016. Heat Content of Natural Gas Consumed. U.S Energy Information Administration. https://www.eia.gov/dnav/ng/ng_cons_heat_a_epg0_vgth_btucf_a.htm, Accessed date: 25 April 2017.

EPA, 2012. Inventory of U.S. Greenhouse Gas Emissions and Sinks: 1990-2010. https://www.epa.gov/ghgemissions/us-greenhouse-gas-inventory-report-archive.

EPA, 2013. Facility Level Information on Greenhouse Gases Tool (FLIGHT). http://go.usa.gov/x8yc8, Accessed date: 28 April 2017.

EPA, 2015a. Greenhouse Gas Reporting Program (GHGRP), Natural Gas Local Distribution Companies. https://ghgdata.epa.gov/ghgp/main.do, Accessed date: 28 April 2017.

EPA, 2015b. Inventory of U.S. Greenhouse Gas Emissions and Sinks: 1990-2013 Washington, D.C. https://www.epa.gov/ghgemissions/us-greenhouse-gas-inventory-report-archive.

EPA, 2017. Inventory of U.S. Greenhouse Gas Emissions and Sinks: 1990-2015, Washington, D.C. https://www.epa.gov/ghgemissions/inventory-us-greenhouse-gas-emissions-and-sinks-1990-2015.

Fiore, A.M., West, J.J., Horowitz, L.W., Naik, V., Schwarzkopf, M.D., 2008. Characterizing the tropospheric ozone response to methane emission controls and the benefits to climate and air quality. J. Geophys. Res. Atmos. 113, D08307. http://dx.doi.org/10.1029/2007jd009162.

Gallagher, M.E., Down, A., Ackley, R.C., Zhao, K., Phillips, N., Jackson, R.B., 2015. Natural gas pipeline replacement programs reduce methane leaks and improve consumer safety. Environ. Sci. Technol. Lett. 2, 286–291. http://dx.doi.org/10.1021/acs.estlett.5b00213.

Hausmann, P., Sussmann, R., Smale, D., 2016. Contribution of oil and natural gas production to renewed increase in atmospheric methane (2007–2014): top–down estimate from ethane and methane column observations. Atmos. Chem. Phys. 16, 3227–3244. http://dx.doi.org/10.5194/acp-16-3227-2016.

Helmig, D., Rossabi, S., Hueber, J., Tans, P., Montzka, S.A., Masarie, K., Thoning, K., Plass-Duelmer, C., Claude, A., Carpenter, L.J., Lewis, A.C., Punjabi, S., Reimann, S., Vollmer, M.K., Steinbrecher, R., Hannigan, J.W., Emmons, L.K., Mahieu, E., Franco, B., Smale, D., Pozzer, A., 2016. Reversal of global atmospheric ethane and propane trends largely due to US oil and natural gas production. Nature Geosci. 9, 490–495. http://dx.doi.org/10.1038/ngeo2721.

Hendrick, M.F., Ackley, R., Sanaie-Movahed, B., Tang, X., Phillips, N.G., 2016. Fugitive methane emissions from leak-prone natural gas distribution infrastructure in urban environments. Environ. Pollut. 213, 710–716. http://dx.doi.org/10.1016/j.envpol.2016.01.094.

Hesterberg, T.W., Lapin, C.A., Bunn, W.B., 2008. A comparison of emissions from vehicles fueled with diesel or compressed natural gas. Environ. Sci. Technol. 42, 6437–6445. http://dx.doi.org/10.1021/es071718i.

Jackson, R.B., Down, A., Phillips, N.G., Ackley, R.C., Cook, C.W., Plata, D.L., Zhao, K., 2014. Natural gas pipeline leaks across Washington, DC. Environ. Sci. Technol. 48, 2051–2058. http://dx.doi.org/10.1021/es404474x.

Jahjah, M., Jiang, W., Sanchez, N.P., Ren, W., Patimisco, P., Spagnolo, V., Herndon, S.C., Griffin, R.J., Tittel, F.K., 2014. Atmospheric CH4 and N2O measurements near Greater Houston area landfills using a QCL-based QEPAS sensor system during DISCOVER-AQ 2013. Opt. Lett. 39, 957–960. http://dx.doi.org/10.1364/ol.39.000957.

Kirschke, S., Bousquet, P., Ciais, P., Saunois, M., Canadell, J.G., Dlugokencky, E.J., Bergamaschi, P., Bergmann, D., Blake, D.R., Bruhwiler, L., Cameron-Smith, P., Castaldi, S., Chevallier, F., Feng, L., Fraser, A., Heimann, M., Hodson, E.L., Houweling, S., Josse, B., Fraser, P.J., Krummel, P.B., Lamarque, J.-F., Langenfelds, R.L., Le Quere, C., Naik, V., O'Doherty, S., Palmer, P.I., Pison, I., Plummer, D., Poulter, B., Prinn, R.G., Rigby, M., Ringeval, B., Santini, M., Schmidt, M., Shindell, D.T., Simpson, I.J., Spahni, R., Steele, L.P., Strode, S.A., Sudo, K., Szopa, S., van der Werf, G.R., Voulgarakis, A., van Weele, M., Weiss, R.F., Williams, J.E., Zeng, G., 2013. Three decades of global methane sources and sinks. Nature Geosci. 6, 813–823. http://dx.doi.org/10.1038/ngeo1955.

Lamb, B.K., Cambaliza, M.O.L., Davis, K.J., Edburg, S.L., Ferrara, T.W., Floerchinger, C., Heimburger, A.M.F., Herndon, S., Lauvaux, T., Lavoie, T., Lyon, D.R., Miles, N., Prasad, K.R., Richardson, S., Roscioli, J.R., Salmon, O.E., Shepson, P.B., Stirm, B.H., Whetstone, J., 2016. Direct and indirect measurements and modeling of methane emissions in indianapolis, Indiana. Environ. Sci. Technol. 50, 8910–8917. http://dx.doi.org/10.1021/acs.est.6b01198.

Lamb, B.K., Edburg, S.L., Ferrara, T.W., Howard, T., Harrison, M.R., Kolb, C.E., Townsend-Small, A., Dyck, W., Possolo, A., Whetstone, J.R., 2015. Direct measurements show decreasing methane emissions from natural gas local distribution systems in the United States. Environ. Sci. Technol. 49, 5161–5169. http://dx.doi.org/10.1021/es505116p.

McKain, K., Down, A., Raciti, S.M., Budney, J., Hutyra, L.R., Floerchinger, C., Herndon, S.C., Nehrkorn, T., Zahniser, M.S., Jackson, R.B., Phillips, N., Wofsy, S.C., 2015. Methane emissions from natural gas infrastructure and use in the urban region of Boston, Massachusetts. Proc. Natl. Acad. Sci. U.S.A 112, 1941–1946. http://dx.doi.org/10.1073/pnas.1416261112.

Michot Foss, M., 2004. Interstate Natural Gas Quality Specifications and Interchangeability. Center for Energy Economics, Sugar Land, TX. http://www.beg.utexas.edu/energyecon/GlobalGas-LNG/documents/CEE_Interstate_Natural_Gas_Quality_Specifications_and_Interchangeability.pdf.

Mitchell, A.L., Tkacik, D.S., Roscioli, J.R., Herndon, S.C., Yacovitch, T.I., Martinez, D.M., Vaughn, T.L., Williams, L.L., Sullivan, M.R., Floerchinger, C., Omara, M., Subramanian, R., Zimmerle, D., Marchese, A.J., Robinson, A.L., 2015. Measurements of methane emissions from natural gas gathering facilities and processing plants: measurement results. Environ. Sci. Technol. 49, 3219–3227. http://dx.doi.org/10.1021/es5052809.

Phillips, N.G., Ackley, R., Crosson, E.R., Down, A., Hutyra, L.R., Brondfield, M., Karr, J.D., Zhao, K., Jackson, R.B., 2013. Mapping urban pipeline leaks: methane leaks across Boston. Environ. Pollut. 173, 1–4. http://dx.doi.org/10.1016/j.envpol.2012.11.003.

PHMSA, 2016a. Distribution, Transmission & Gathering, LNG, and Liquid Accident and Incident Data, Natural Gas Distribution Incident Data 2009-2016. https://www.phmsa.dot.gov/pipeline/library/data-stats/distribution-transmission-and-gathering-lng-and-liquid-accident-and-incident-data, Accessed date: 20 April 2017.

PHMSA, 2016b. Gas distribution Pipeline Miles. Pipeline Replament Updates, Bare Steel Inventory and Cast and Wrought Iron Inventory. https://opsweb.phmsa.dot.gov/pipeline_replacement/, Accessed date: 20 April 2017.

Schoell, M., 1980. The hydrogen and carbon isotopic composition of methane from natural gases of various origins. Geochem. Cosmochim. Acta 44, 649–661. http://dx.doi.org/10.1016/0016-7037(80)90155-6.

Simpson, I.J., Sulbaek Andersen, M.P., Meinardi, S., Bruhwiler, L., Blake, N.J., Helmig, D., Rowland, F.S., Blake, D.R., 2012. Long-term decline of global atmospheric ethane concentrations and implications for methane. Nature 488, 490–494. http://dx.doi.org/10.1038/nature11342.

Stanley, E.H., Casson, N.J., Christel, S.T., Crawford, J.T., Loken, L.C., Oliver, S.K., 2016. The ecology of methane in streams and rivers: patterns, controls, and global significance. Ecol. Monogr. 86, 146–171. http://dx.doi.org/10.1890/15-1027.

Subramanian, R., Williams, L.L., Vaughn, T.L., Zimmerle, D., Roscioli, J.R., Herndon, S.C., Yacovitch, T.I., Floerchinger, C., Tkacik, D.S., Mitchell, A.L., Sullivan, M.R., Dallmann, T.R., Robinson, A.L., 2015. Methane emissions from natural gas compressor stations in the transmission and storage sector: measurements and comparisons with the EPA greenhouse gas reporting program protocol. Environ. Sci. Technol. 49, 3252–3261. http://dx.doi.org/10.1021/es5060258.

Turner, B., 1994. Workbook of Atmospheric Dispersion Estimates: an Introduction to Dispersion Modeling, second ed. Lewis Publishing/CRC Press, Florida.

United States Census Bureau, 2014. 2010 – 2014 American Community Survey. U.S. Census Bureau's American Community Survey Office, 2014. https://www.census.gov/programs-surveys/acs/technical-documentation/table-and-geography-changes/2014/5-year.html, Accessed date: 15 March 2016.

von Fischer, J.C., Cooley, D., Chamberlain, S., Gaylord, A., Griebenow, C.J., Hamburg, S.P., Salo, J., Schumacher, R., Theobald, D., Ham, J., 2017. Rapid, vehicle-based identification of location and magnitude of urban natural gas pipeline leaks. Environ. Sci. Technol. 51, 4091–4099. http://dx.doi.org/10.1021/acs.est.6b06095.

Wennberg, P.O., Mui, W., Wunch, D., Kort, E.A., Blake, D.R., Atlas, E.L., Santoni, G.W., Wofsy, S.C., Diskin, G.S., Jeong, S., Fischer, M.L., 2012. On the sources of methane to the Los Angeles atmosphere. Environ. Sci. Technol. 46, 9282–9289. http://dx.doi.org/10.1021/es301138y.

Xiao, Y., Logan, J.A., Jacob, D.J., Hudman, R.C., Yantosca, R., Blake, D.R., 2008. Global budget of ethane and regional constraints on U.S. sources. J. Geophys. Res. Atmos. 113, D21306. http://dx.doi.org/10.1029/2007jd009415.

Yacovitch, T.I., Herndon, S.C., Roscioli, J.R., Floerchinger, C., McGovern, R.M., Agnese, M., Pétron, G., Kofler, J., Sweeney, C., Karion, A., Conley, S.A., Kort, E.A., Nähle, L., Fischer, M., Hildebrandt, L., Koeth, J., McManus, J.B., Nelson, D.D., Zahniser, M.S., Kolb, C.E., 2014. Demonstration of an ethane spectrometer for methane source identification. Environ. Sci. Technol. 48, 8028–8034. http://dx.doi.org/10.1021/es501475q.

Ye, W., Li, C., Zheng, C., Sanchez, N.P., Gluszek, A.K., Hudzikowski, A.J., Dong, L., Griffin, R.J., Tittel, F.K., 2016. Mid-infrared dual-gas sensor for simultaneous detection of methane and ethane using a single continuous-wave interband cascade laser. Optic Express 24, 16973–16985. http://dx.doi.org/10.1364/oe.24.016973.

Zavala-Araiza, D., Allen, D.T., Harrison, M., George, F.C., Jersey, G.R., 2015. Allocating methane emissions to natural gas and oil production from shale formations. ACS Sustain. Chem. Eng. 3, 492–498. http://dx.doi.org/10.1021/sc500730x.